Benchmarking Thermochemistry-Coupled Radionuclide Release in Molten Salt Reactors: cGEMS vs OpenFOAM-GEMS

Dowon Lee[a], Juhyeong Lee[a], JinHo Song[a], Sung Joong Kim[*a,b]
[a]*Department of Nuclear Engineering, Hanyang University*
222 Wangsimni-ro, Seongdong-gu, Seoul 04763, Republic of Korea
[b]*Institute of Nano Science and Technology, Hanyang University*
222 Wangsimni-ro, Seongdong-gu, Seoul 04763, Republic of Korea
[*]*Corresponding author: sungjkim@hanyang.ac.kr*

Keywords : Molten Salt Reactor, OpenFOAM, GEMS, Mechanistic source term, Fission product release

1. Introduction

Molten Salt Reactors (MSRs) are gaining significant attention due to their unique inherent safety characteristics. However, their deployment requires a novel regulatory methodology. Traditional Light Water Reactor (LWR) source term prescriptions are inherently incompatible with MSRs. Specifically, the highly conservative assumptions of TID-14844 and the solid fuel-based transport mechanisms of NUREG-1465 cannot adequately capture the distinct behaviors of liquid fuel systems [1-2].

Unlike the cladding failure mechanisms that dictate radionuclide release in LWRs, MSRs are governed by different physical phenomena. In events such as a salt spill, the release of the source term is driven by the evaporation of fission products and actinides dissolved within the liquid salt pool. Because of these distinct release mechanisms, advanced reactor licensing is evolving toward Technology-Inclusive, Risk-Informed, and Performance-Based (TI-RIPB) approaches. Consequently, mechanistic source term (MST) evaluations are essential to accurately model the vaporization and physical transport of these radionuclides [3].

To support MSR MST analysis, recent studies couple equilibrium thermochemistry with transport and release models. A representative implementation is cGEMS, developed at the Paul Scherrer Institute (PSI), which couples the MELCOR system code with the Gibbs free energy minimization solver (GEMS). While such system codes efficiently evaluate radionuclide release, they typically rely on lumped-parameter assumptions and correlation-based approaches for interfacial mass transfer.

To resolve spatial variations that influence interfacial transport, a Computational Fluid Dynamics (CFD) framework, OpenFOAM-GEMS, was developed. Accordingly, calculations were performed by benchmarking a representative cGEMS test case [4]. The comparison evaluates radionuclide release predictions, equilibrium vapor pressures, and mass transfer coefficients to analyze the implications of spatially resolved transport modeling for MSR MST evaluations.

2. Modeling and Methodology

2.1 Overview of the coupled frameworks

The architecture and preliminary verification of the OpenFOAM-GEMS solver are detailed in a previous study [5]. The coupled framework employs OpenFOAM to resolve transient thermal-fluid fields, while GEMS evaluates the localized chemical equilibrium of the defined chemical system based on its elemental inventory.

A comparative assessment against cGEMS is performed to evaluate the physical consistency of the mechanistic evaporation modeling. The focus remains on verifying the vaporization behavior at the salt-gas interface within the spatially resolved framework. Section 2.2 details the derivation of equilibrium vapor pressures and mass transfer coefficients, which serve as the primary drivers for the evaporation model. Section 2.3 describes the benchmarking parameters and the numerical method used to align the physical conditions between the two solvers.

2.2 Radionuclide Release Modeling

In both cGEMS and OpenFOAM-GEMS, volatilization-driven release is evaluated using the interfacial mass transfer formulation. The interfacial molar flux of species i, $\dot{n}_i''$, is driven by the gradient between the equilibrium vapor pressure at the interface and the bulk gas partial pressure:

$$\dot{n}_i'' = \frac{k_i}{RT_{surf}}\left(P_{i,vap} - P_{i,\infty}\right) \quad (1)$$

where k_i is the mass transfer coefficient, R is the universal gas constant, and T_{surf} is the interface temperature. Here $P_{i,vap}$ denotes the equilibrium vapor pressure obtained from thermochemical equilibrium calculations, and $P_{i,\infty}$ represents the bulk gas partial pressure. Since the identical mass transfer model is employed in both frameworks, differences in predicted release are primarily governed by the evaluation of k_i and $P_{i,vap}$.

2.2.1 Mass transfer coefficient calculation

Both frameworks employ the Chilton-Colburn analogy to relate heat and mass transfer, though the implementations differ. In cGEMS, MELCOR computes the pool-to-atmosphere heat transfer coefficient, h, using Reynolds-number-based empirical correlations under a lumped-parameter representation. The resulting h is converted to a reference mass transfer coefficient, k_{ref}, and scaled for each species as

$$k_{ref} = \frac{h}{\rho C_p}\left(\frac{Sc_{ref}}{Pr}\right)^{-2/3} \quad (2)$$

$$k_i = k_{ref}\left(\frac{D_{i,g}}{D_{ref,g}}\right)^{2/3} \quad (3)$$

where $D_{i,g}$ is the binary gas-phase diffusivity of species i and $D_{ref,g}$ is the diffusivity of the MELCOR reference pair. In contrast, OpenFOAM-GEMS, derives k_i from CFD-resolved interfacial boundary layers using the local heat transfer coefficient h_{local}, without an intermediate standard-pair scaling:

$$k_i = \frac{h_{local}}{\rho C_p}\left(\frac{Sc_i}{Pr}\right)^{-2/3} \quad (4)$$

2.2.2 Equilibrium vapor pressure evaluation

Differences also exist in the evaluation of the equilibrium vapor pressure, $P_{i,vap}$. Both frameworks utilize GEMS to account for the non-ideality of molten salt thermochemistry. In cGEMS, MELCOR requires $P_{i,vap}$ in a parameterized form. Therefore, GEMS outputs are represented by an Antoine-type expression over the prescribed temperature range,

$$\log_{10}(P_{i,vap}) = B_i - \frac{A_i}{T} + C_i \log_{10}(T) \quad (5)$$

The fitted coefficients are provided to MELCOR. In contrast, OpenFOAM-GEMS utilizes $P_{i,vap}$ obtained directly from GEMS at the local interface temperature. In the present benchmark, this parameterization is treated as an implementation detail and is not expected to dominate the observed release differences.

2.3 Simulation setup and benchmark definition

The benchmark scenario is based on the Molten Salt Fast Reactor (MSFR) pool-release case, which evaluates radionuclide release following a salt spill accident [4]. The computational domain represents an MSFR containment where a spilled molten salt pool at the bottom interacts with an overlying inert nitrogen atmosphere in a 20 m-high cylindrical vessel. As illustrated in Figure 1, the upper 5 m of the gas region is modeled as a heat exchanger (HX) zone, with the boundary temperature fixed at 500 K to provide a continuous heat sink.

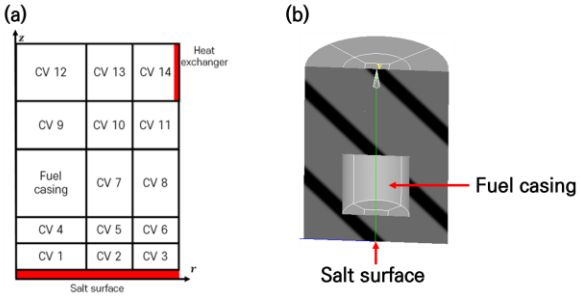

Fig. 1. Modeling domain for the MSR pool-release case: (a) cGEMS control volume, (b) OpenFOAM-GEMS geometry

To resolve interfacial transport between the salt pool and the gas region, conjugate heat transfer CFD simulations are performed using chtMultiRegionFoam (OpenFOAM v2406). Consistent with the reference study, the molten salt pool is modeled as a stationary solid region, while the overlying atmosphere is treated as a fluid region. The domain is discretized using a structured hexahedral O-grid mesh with 132,000 cells generated in SALOME 9.12 (Figure 2).

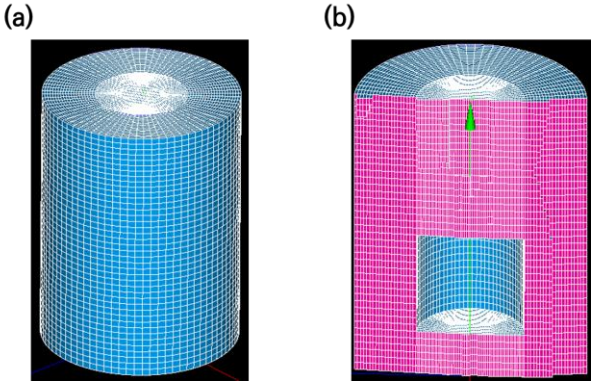

Fig. 2. CFD mesh used in OpenFOAM-GEMS for the MSFR containment model: (a) full mesh, (b): cut view

Initial and boundary conditions match those of the reference study. The system is initialized at 500 K and 101,325 Pa, with elemental inventories derived from EQ0LD simulation results. During the 12,000 s transient, the spilled pool undergoes a heat-up phase driven by decay heat, reaching 1,500 K. This temperature increase drives the volatilization of fission products into the containment atmosphere. The key simulation parameters and initial compositions are summarized in Tables I and II.

Table I: Major parameters for OpenFOAM calculation

Parameters	Values
Simulation	
Solver	chtMultiRegionFoam
Turbulence model	buoyant k-epsilon (Containment)
Time step	200 s
Iteration and Discretization	
Iteration algorithm	PIMPLE (Pressure-Velocity coupling algorithm)
Smoother	symGaussSeidel
Time term	Euler
Gradient term	Gauss linear
Interpolation	Linear

Radiation Model	
Model	fvDOM

Boundary conditions	**Values**
Temperature boundary conditions	
Top	zeroGradient
HX	fixedValue (500K)
Fuelcase	zeroGradient
Fuelsalt	uniformedFixedValue (500 to 1500 K, 12000 s)
Velocity boundary conditions	
Top HX Fuelcase	noSlip
Pressure boundary condition	
Top	fixedFluxPressure (1 atm)
HX	fixedFluxPressure (1 atm)
Fuelcase	fixedFluxPressure (1 atm)
Fuelsalt	calculated

Table II: Initial elemental composition for GEMS calculation

Element	Symbol	Molar amount (mol)
Argon	Ar	1.000E-08
Cesium	Cs	8.276E+01
Fluorine	F	1.410E+06
Iodine	I	4.728E-01
Lithium	Li	6.800E+05
Thorium	Th	1.461E+05
Uranium	U	3.634E+04
Nitrogen	N	2.204E+04

3. Result and Discussion

3.1 Overview of Release model comparison

As described in Section 2.2, cGEMS and OpenFOAM-GEMS compute volatilization-driven release using the same interfacial mass transfer formulation (Eq. (1)). Under the formulation, the release rate is primarily governed by two quantities: the species mass transfer coefficient k_i, and the equilibrium vapor pressure $P_{i,vap}$.

To compare the variables individually, the analysis is divided into two parts. Section 3 compares k_i and its impact on transient release, while Section 3.3 compares the equilibrium vapor pressure.

3.2 Mass transfer coefficient

Figure 3 presents the time evolution of the normalized mass transfer coefficient, $k_g(t)/k_g(t_0)$, with $t_0 = 200\ s$, predicted by cGEMS and OpenFOAM-GEMS. Opposite trends are observed: $k_g(t)/k_g(t_0)$ decreases continuously in cGEMS, whereas OpenFOAM-GEMS increases and then reaches a saturated state. LiF is used as a representative species, and other species show similar normalized trends. At 30,000 s, OpenFOAM-GEMS predicts $k_g = 1.23 \times 10^{-2}\ m/s$, about 4.4 times higher than $2.81 \times 10^{-3}\ m/s$ in cGEMS.

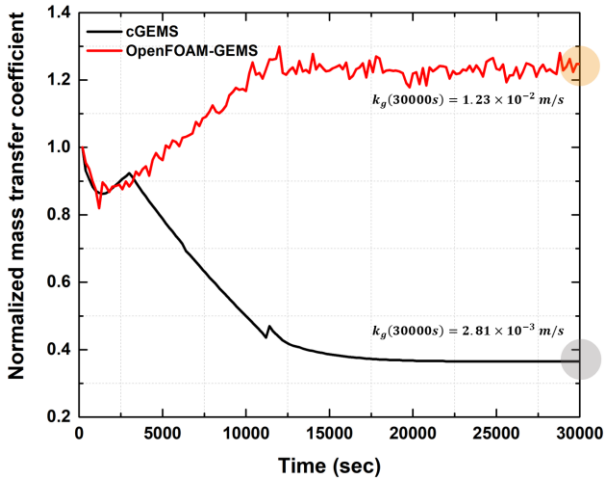

Fig. 3. Normalized mass transfer coefficient time evolution

In cGEMS, the declining trend follows the multiplicative structure of Eq. (3). From 200 to 30,000 s, k_{ref} and $(D_{i,g}/D_{ref,g})^{2/3}$ decrease by factors of 0.469 and 0.773, respectively, yielding an overall reduction of $k_g(t)/k_g(t_0)$ to 0.363 of its initial value. Conversely, in OpenFOAM-GEMS, the $1/\rho C_p$ term decreases to 0.589, while h_{local} and $(Sc_i/Pr)^{-2/3}$ increase by factors of 1.273 and 1.575. The combined effect yields a net increase of k_g by a factor of 1.18, consistent with the saturated state observed in Figure 3.

Based on the heat-mass transfer analogy (Eqs. (2) and (4)), k_g is tied to the Sherwood number, which is coupled to the Nusselt number. Therefore, discrepancies in interfacial heat transfer evaluation propagate directly to k_g. In cGEMS, the heat transfer coefficient is obtained from MELCOR's Reynolds-number-based correlation under a lumped parameter HS treatment. In contrast, OpenFOAM-GEMS dervies h_{local} from CFD-resolved thermal and velocity boundray layers at the molten-salt atmosphere interface. Figure 4 compares the interfacial heat transfer coefficients predicted by the two frameworks.

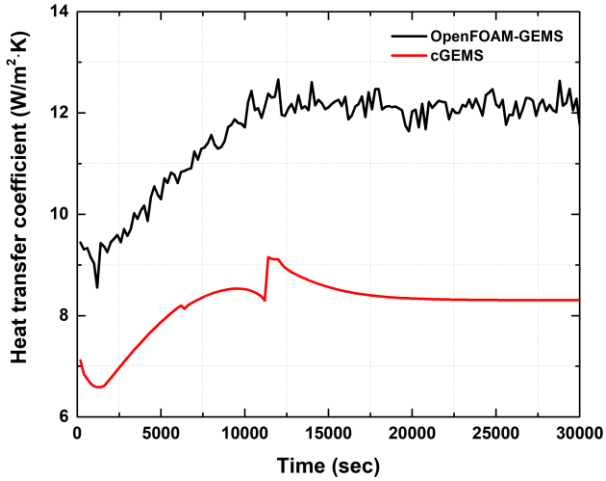

Fig. 4. Interfacial heat transfer coefficient predicted by cGEMS and OpenFOAM-GEMS

3.3 Evaporation driving force

This subsection evaluates the thermodynamic trend for evaporation by comparing equilibrium vapor pressure predicted by GEMS with the gas-phase partial pressure. To enable a code-to-code comparison, a normalized driving force is introduced and used to characterize the time evolution of evaporation potential for representative species. The normalized driving force definition is given in Eq. (6).

$$\Phi_i = \max\left(0, \frac{p_{eq,i} - p_{partial,i}}{p_{eq,i}}\right) = \max\left(0, 1 - \frac{p_{partial,i}}{p_{eq,i}}\right) \quad (6)$$

Figure 5 presents Φ_i for LiF, ThF_4, CsF, and Li_3F_3 from OpenFOAM-GEMS and cGEMS. LiF and ThF_4 stay at $\Phi_i \approx 1$ in cGEMS because vapor is converted to aerosol, keeping $p_{partial,i} \approx 0$. In OpenFOAM-GEMS, an aerosol formation mechanism is not implemented, so the vapor-phase partial pressure is not reduced by an aerosol sink. Consequently, Φ_i decreases only as the gas phase approaches saturation. During the temperature increase, CsF in both codes reaches $\Phi_i \approx 0$, indicating that $p_{partial,i}$ approaches $p_{eq,i}$ (Eq.(7)). Such behavior is consistent with non-ideal molten salt effects, where salt composition changes reduce CsF activity and limit the rise of $p_{eq,i}$ despite increasing temperature. After 12,000 s, the temperature reaches 1,500 K and the subsequent Φ_i evolution is controlled by sink mechanisms. In cGEMS, continuous transport from the evaporation control volumes (CV1 – CV3) to the connected control volumes above (CV4 – CV6) acts as an additional sink that sustains undersaturation and delays the decay of Φ_i. In OpenFOAM-GEMS, such transport removal is not modeled, so Φ_i remains near 0 once $p_{partial,i}$ has approached $p_{eq,i}$.

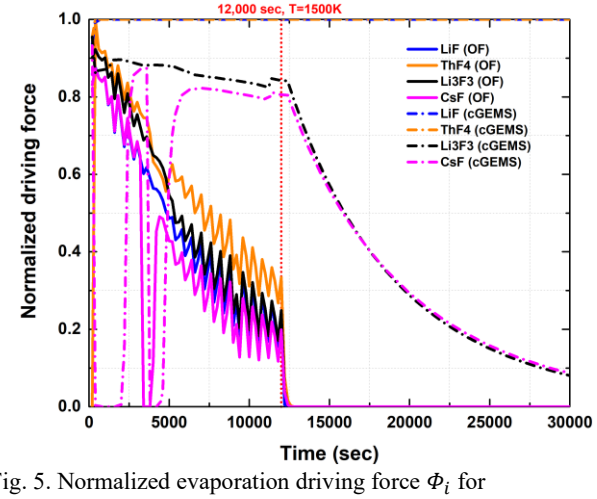

Fig. 5. Normalized evaporation driving force Φ_i for representative species (OpenFOAM-GEMS vs. cGEMS)

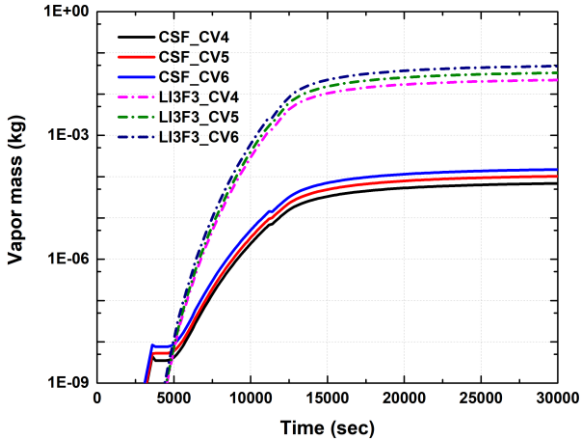

Fig. 6. cGEMS vapor mass of CsF and Li_3F_3 in CV4 - CV6

3.4 Cumulative released mass

Table III compares cumulative released masses at 30,000 s. The differences are consistent with the combined effects of k_g (Section 3.2) and the evaporation driving force Φ_i (Section 3.3). In cGEMS, aerosol conversion acts as a dominant sink for aerosol-forming species (LiF, ThF_4, UF_4, Li_2F_2, I), as indicated by $f_{aer} \approx 1$ in Table III. For the remaining species, vapor removal is primarily driven by control volume transport from the evaporation control volumes (CV1 – CV3) to the connected control volumes above (CV4 – CV6; Fig. 6), as reflected by the low vapor masses retained in CV1 – CV3. These sink terms largely explain the discrepancy, and aerosol formation and control volume transport are planned for future development of OpenFOAM-GEMS.

Table III: Cumulative released mass at 30,000 s

Species	OpenFOAM-GEMS (kg)	cGEMS vapor (CV1 - 3)(kg)	cGEMS total (kg)	f_{aer}
CsI	2.68E-06	9.09E-05	1.13E-03	0.00
CsF	4.48E-04	3.19E-04	3.96E-03	0.00
LiF	6.50E-01	0.00E+00	8.92E+00	1.00
ThF_4	1.32E+00	0.00E+00	1.42E+01	1.00
LiI	1.87E-04	1.08E-04	1.34E-03	0.00
UF_4	4.36E-01	0.00E+00	4.75E+00	1.00
Li_2F_2	4.96E-01	0.00E+00	6.14E+00	1.00
Li_3F_3	1.49E-01	1.02E-01	1.26E+00	0.00
Li	1.88E-07	7.57E-08	9.41E-07	0.00
ThF_3	3.95E-02	1.22E-02	1.52E-01	0.00
UF_3	2.56E-06	7.84E-07	9.74E-06	0.00
I	3.86E-04	7.12E-07	1.47E-02	0.99

4. Conclusions

This study developed and benchmarked OpenFOAM-GEMS, a CFD-thermochemistry coupled framework for volatilization-driven source term evaluation in MSR accident scenarios. The framework couples OpenFOAM with GEMS to compute non-ideal equilibrium vapor pressures and chemical speciation, and applies an

interfacial mass-transfer formulation. consistent with cGEMS for a code-to-code comparison using an MSFR pool-release benchmark. Key findings include:

- ✓ Mass transfer coefficient: OpenFOAM-GEMS predicts an increasing k_g that reaches a saturated, while cGEMS predicts a decreasing k_g, resulting in a 4.4 times differences at the end of simulation. The discrepancy is attributed to differences in interfacial heat transfer treatment (h)
- ✓ Evaporation driving force: The normalized driving force, Φ_i captures the balance between $p_{eq,i}$ and $p_{partial,i}$. In cGEMS, aerosol forming species maintain $\Phi_i \approx 1$ due to vapor to aerosol conversion. CsF reaches $\Phi_i \approx 0$ during heat-up in both codes, consistent with non-ideal molten salt effect under composition change.
- ✓ Cumulative release: Differences in cumulative released mass are driven by sink pathways present in cGEMS. The dominant sink mechanisms in cGEMS are aerosol conversion and control volume transport modeling, which are not included in the current OpenFOAM-GEMS scope.

Overall, the benchmark confirms consistent thermochemcial driving-force trend between the two frameworks, while identiying system level sink modeling as the primary gap for achieving agreement in cumulative released mass. Future work will implement aerosol dynamics and control volume transport modeling in OpenFOAM-GEMS to enable system-consistent released mass prediction.

Acknowledgements

This work was supported by the Human Resources Development of the Korea Institute of Energy Technology Evaluation and Planning (KETEP) grant funded by the Korea government Ministry of Knowledge Economy (RS-2024-00439210) and by the Nuclear Safety Research Program through the Korea Foundation of Nuclear Safety (KoFONS) using the financial resource granted by the Nuclear Safety and Security Commission (NSSC) of the Republic of Korea (RS-2025-02312295).

REFERENCES

[1] U.S. Atomic Energy Commission. (1962). *Calculation of distance factors for power and test reactor sites* (TID-14844). U.S. Nuclear Regulatory Commission.
[2] NUREG-1465, “Accident Source Terms for Light Water Nuclear Power Plants”, US NRC, 1995.
[3] U.S. Nuclear Regulatory Commission, "Performance-Based Emergency Preparedness for Small Modular Reactors, Non-Light-Water Reactors, and Non-Power Production or Utilization Facilities," RG 1.242, Draft Rev 0, 2021.
[4] Kalilainen, J., Nichenko, S., & Krepel, J. (2020). Evaporation of materials from the molten salt reactor fuel under elevated temperatures. *Journal of Nuclear Materials, 533*, 152134.
[5] Lee, D., Lee, J., Song, J., & Kim, S. J. (2025, October 30–31). *A coupled OpenFOAM-GEMS framework for simulating fission product release from molten salt reactors*. In *Transactions of the Korean Nuclear Society Autumn Meeting* (Changwon, Republic of Korea).